Journal of Nanostructure in Chemistry (2017) 7:375–387
https://doi.org/10.1007/s40097-017-0248-z

ORIGINAL RESEARCH

Synthesis and comparative studies of $MnFe_2O_4$ nanoparticles with different natural polymers by sol–gel method: structural, morphological, optical, magnetic, catalytic and biological activities

A. Mary Jacintha[1,2] · V. Umapathy[3] · P. Neeraja[4] · S. Rex Jeya Rajkumar[5]

Received: 12 October 2017 / Accepted: 23 November 2017 / Published online: 27 November 2017

Abstract

Nanosized manganese ferrite ($MnFe_2O_4$) particles were prepared by sol–gel method using natural polymers like wheat flour (WF) and potato flour (PF) as surfactants and its structural, morphological, optical and magnetic characteristics were studied by X-ray diffraction (XRD), Fourier Transform Infrared Spectroscopy (FT-IR), scanning electron microscope (SEM), photoluminescence spectroscopy (PL) and vibration sample magnetometer (VSM). Brunauer–Emmett–Teller (BET) surface area test also performed and the results obtained were discussed. The average crystallite size was found to be 23 and 16 nm for WF/$MnFe_2O_4$ and PF/$MnFe_2O_4$ samples, respectively. Magnetic hysteresis loops confirmed the super-paramagnetic behavior for both the samples. For oxidation of benzyl alcohol to benzaldehyde, the catalytic activity of $MnFe_2O_4$ nanoparticles (NPs) was carried out. Antimicrobial and antifungal activity of WF/$MnFe_2O_4$ and PF/$MnFe_2O_4$ samples were investigated against two Gram-positive bacteria (*Staphylococcus aureus*, *Streptococcus pneumoniae*), two Gram-negative bacteria (*Pseudomonas aeruginosa*, *Salmonella paratyphi*) and fungus (*Candida albicans*) using inhibition zone method. Minimum Inhibitory Concentration (MIC) values also calculated to determine susceptibilities of bacteria to drugs and also to evaluate the activity of new antimicrobial agents. The in vitro cytotoxicity of newly synthesized samples were analyzed by MTT assay against MCF-7, A549 and HaCaT cell lines in a dose-dependent fashion. Among these two samples, sample B (using potato flour) shows better response than sample A (using wheat flour) and both the samples were non-toxic to normal cell line. The concentration required to kill 50% of the cell (IC_{50}) was also calculated.

Graphical Abstract

$MnFe_2O_4$ nanoparticles were synthesized by sol–gel method using natural polymers, wheat flour and potato flour, as surfactant. The as-prepared $MnFe_2O_4$ was characterized by XRD, FT-IR, SEM, EDX, PL and VSM analysis. The average crystallite size was found to be 23 and 16 nm for WF/$MnFe_2O_4$ and PF/$MnFe_2O_4$ samples, respectively. Magnetic hysteresis loops confirmed the super-paramagnetic behavior for both the samples. The catalytic activity of $MnFe_2O_4$ nanoparticles (NPs) were carried out for oxidation of benzyl alcohol to benzaldehyde. Biological activities like antimicrobial, antifungal and anticancer activities of the samples were investigated. Among these two samples, PF/$MnFe_2O_4$ shows better response than WF/$MnFe_2O_4$ and both the samples were non-toxic to normal cell line.

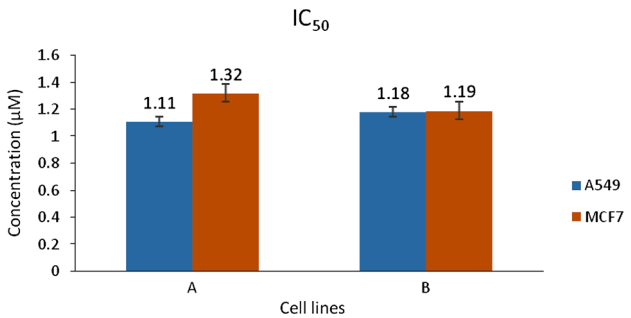

IC_{50} values of WF/$MnFe_2O_4$ (**a**) and PF/$MnFe_2O_4$ (**b**) against A549 and MCF-7 cell lines

Extended author information available on the last page of the article

Keywords Manganese ferrite · Nanoparticles · Natural surfactants · Antimicrobial activity · MIC · Gram-positive bacteria · Gram-negative bacteria · Anticancer · In vitro cytotoxicity

Introduction

Nanomaterials play a vital role in the field of nanomedicine and nanobiotechnology. They can offer a new approach to antibiotic-resistance microbes [1]. In several studies nanoparticles (NPs) can be used as therapeutic tools to treat infections against microbes because of their unique physical, chemical, mechanical and magnetic properties. Due to this, NPs grab attention in the clinical application to produce a variety of new bactericidal agent [2, 3]. The materials in nanoscale can penetrate into bacterial cells and produce toxic oxygen radicals to damage cell membranes of microbes that produce an efficient inhibition bacterial growth [4–7]. Spinel structure ferrite nanoparticles creates a great impact among the science researchers because of its wide applications in magnetic resonance imaging, magnetic storage devices, biotechnology, electronics, magnetic drug delivery [8–10], etc. Magnetic nanoparticles possess excellent super-paramagnetic property due to large surface-to-volume ratio of the nanoparticles and they require super-paramagnetic character at room temperature for many applications [11–14]. Among all the spinel ferrites known today, $MnFe_2O_4$ nanoparticles have high surface area, high saturation magnetization, high mechanical hardness and possess excellent chemical stability [15]. Literature survey reveals that manganese ferrite nanoparticles are synthesized by several methods like traditional ceramic methods, oxalate method, sol–gel, chemical co-precipitation, mechanical ball milling, thermal decomposition, hydrothermal, combustion, and micro emulsion method [16–19].

Out of many methods stated above, sol–gel method is considered to be an appropriate one, whereas innumerable applications are prevalent. World's lightest materials and some toughest ceramics were produced by the scientists using this method. Sol–gel method applications are wide, especially in thin films which are produced by spin or dip coating on a piece of substrate. Glass articles with novel properties can be formed which cannot be created by any other method. Various surfactants were used so far in sol–gel method, but no report is available on the effects of wheat flour (WF) and potato flour (PF) as surfactants. In this study WF and PF were used as surfactants for synthesis of manganese ferrite. The structural, morphological, optical and magnetic properties of $MnFe_2O_4$ (sample A and B) were characterized by XRD, UV–visible spectroscopy, Fourier transform-infrared (FT-IR) spectroscopy, scanning electron microscope (SEM), energy dispersive X-ray (EDX) spectroscopy, photoluminescence (PL) spectra and VSM measurements. Benzyl alcohol oxidation catalytic activity test was carried out and the product formed was characterized by gas chromatography (GC).

The antimicrobial activity of nanoparticles depends on the size and morphologies of the samples [20, 21]. So far limited information is available on the antimicrobial properties of $MnFe_2O_4$ NPs. In this present work the antimicrobial activity of sample A and sample B were investigated against two Gram-positive bacteria (*Staphylococcus aureus*, *Streptococcus pneumoniae*), two Gram-negative bacteria (*Pseudomonas aeruginosa*, *Salmonella paratyphi*) and fungus (*Candida albicans*). Now-a-days the contribution of cancer to human mortality is also a major threat to human kind. In 2008, the International Agency for Research on cancer estimated that India represents about 8% of cancer death globally and about 6% of death in India [22]. So no doubt that, cancer is a threat. Shocking information from the recent studies is that, the numbers of cancer deaths are increasing and it will increase more in future. It is predicted to increase 11 million in 2030. Lung cancer is major of all and it is due to the high incidence rapid progression and poor prognosis [23]. Currently chemotherapy has been used to cure cancer. At the same time side-effects should also taken into account for some anti-tumor chemotherapeutics. Thus, investigation of new chemicals for treatment of cancer is necessary. Various types of nanoparticles synthesized from inorganic as well as organic materials shows potential applications in cancer therapy [24, 25]. The remarkable heating effects of magnetic nanoparticles used as drug delivery structures, provide an opportunity to target tumor cells [26]. The effectiveness of chemotherapy treatment is restricted, because most of the drugs used to treat cancer exhibit toxicity to both tumor and normal cells. So understanding of nanoparticles and their toxicity is very important. In this study, an attempt was made to evaluate the in vitro cytotoxic activity of the newly synthesized compounds against human lung carcinoma (A549) and human breast carcinoma (MCF-7). Keratinocytes (HaCaT) cell was used as normal cell line.

Materials and methods

Chemicals and reagents used

Manganese ferrite nanoparticles were synthesized using ferric nitrate ($Fe(NO_3)_3{\cdot}9H_2O$), manganese nitrate ($Mn(NO_3)_2{\cdot}4H_2O$) and NaOH. Potato flour and wheat flour are used as surfactants. All these reagents used in the experiments were obtained from Merck India and they

are analytically pure (AR grade around 99.9% pure), so it was used without any further purification.

Synthesis of manganese ferrite nanoparticles

An appropriate amount of manganese nitrate ($Mn(NO_3)_2{\cdot}4H_2O$) (6.2 g), ferric nitrate ($Fe(NO_3)_3{\cdot}9H_2O$) (20.1 g) and sodium hydroxide (4 g) were dissolved separately in a beaker with 100 ml of deionizer water and stirred for 15 min to obtain clear solution and mixed predominantly. The polymer solution was made by mixing 20 g of wheat flour with 100 ml of deionized water with a help of a magnetic stirrer. The metal nitrate solutions and sodium hydroxide solution were added to polymer solution slowly with constant stirring at 50 °C to form sol. This sol was then heated slowly to 90 °C under constant stirring to obtain a wet gel. Then the wet gel product was dried over in hot air oven for 2 days. Then it was calcinated at 600 °C for 2 h at a heating rate of 10 °C/min. It was crushed and powdered in a mortar for 30 min. This powdered sample was labeled as sample A ($MnFe_2O_4$). In another experiment sample B ($MnFe_2O_4$) also synthesized, following the same procedure, but replacing wheat flour with potato flour. The wheat flour and potato flour used were commercial one, which is composed of various materials such as moisture, protein, fat, carbohydrate, fiber and ash.

Characterization techniques

The characterization of newly synthesized sample A and B nanopowders were conducted using various techniques to identify the phase formation, crystal size, distribution and to explore other parameters of interest. The structural characterizations of both samples were studied using PANalytical X'pert pro X-ray diffractometer equipped with Cu-Kα radiation of wave length $\lambda = 1.5418$ Å. Surface functional groups were analyzed by Perkin Elmer FT-IR spectrometer. Morphological studies and energy dispersive X-ray analysis (EDX) of $MnFe_2O_4$ NPs have been performed with FEI Quanta FEG 200 high resolution scanning electron microscopy (HR-SEM). The surface area was derived from N_2 adsorption–desorption isotherms using Quantachrome Corp. Nova-1000 gas sorption analyzer with liquid nitrogen at 77 K. The UV–visible diffuse reflectance spectrum (DRS) was recorded using Cary 100 UV–visible spectrophotometer. Using Varian Cary Eclipse Fluorescence Spectrophotometer, PL properties were recorded in room temperature. The magnetization measurements were performed using VSM-LakeShore 7304 model Vibrating Sample Magnetometer with a maximum field of 15,000 Gauss at room temperature.

Catalytic test

Both WF/$MnFe_2O_4$ and PF/$MnFe_2O_4$ nanopowders were used as catalyst for the oxidation of benzyl alcohol. It was done in a batch reactor under atmospheric conditions. 10 mol of oxidant (H_2O_2) was added along with 1 g of nanosized catalysts (Sample A and B) and the contents were heated at 80 °C in an acetonitrile medium for 10 h in a three necked round bottom flask equipped with a reflux condenser and thermometer. After the reaction, the oxidized products were collected and studied using Agilent GC spectrometer. DB wax column of length 30 mm was used as capillary column and helium gas was used as the carrier gas for this study. The oxidized products obtained were calculated by the following formulae,

$$\text{Conversion}(\%) = \frac{\text{Std peak area} - \text{Sample peak area}}{\text{Std peak area}} \times 100 \quad (1)$$

$$\text{Selectivity}(\%) = \frac{\text{Sample peak area}}{\text{Total peak area}} \times 100. \quad (2)$$

Antimicrobial activity

Antimicrobial activity of newly synthesized $MnFe_2O_4$ nanoparticles were examined using Agar well diffusion method against two Gram-positive bacteria (*Staphylococcus aureus*, *Streptococcus pneumoniae*), two Gram-negative bacteria (*Pseudomonas aeruginosa*, *Salmonella paratyphi*) and fungus (*Candida albicans*). All the tested pathogens were obtained from Microbial Type Culture Collection (MTCC), Chandigarh, India and Microbiological laboratory, Coimbatore, Tamil Nadu, India. Stock solution was prepared by dissolving 1 mg of $MnFe_2O_4$ nanoparticles (WF/$MnFe_2O_4$ and PF/$MnFe_2O_4$) in 1 ml of pure dimethyl sulfoxide (DMSO) (0.1% w/v) and stored at 4 °C. The bacterial and fungal cultures were incubated for 24 h at 37 °C on nutrient agar and potato dextrose agar, respectively. Bacterial strains were grown in Mueller-Hinton agar plates, whereas fungal strains were grown in Potato Dextrose agar plates. A set of three concentrations (25, 50 and 100 µg/ml of $MnFe_2O_4$ nanoparticles) were used in this study. Gentamycin was used as positive control for bacteria and Ketaconozole was used as positive control for fungus. For all the bacteria and fungi strains, overnight cultures grown in broth were adjusted to an inoculum size of 10^6 CFU/ml for inoculation of the agar plates. These cultures were uniformly spread on Mueller-Hinton agar plates (Bacteria) and Potato Dextrose Agar plates (Fungi) separately. Four wells of uniform sizes were made with a cork borer in each organism plate; 25, 50 and 100 µg/ml

$MnFe_2O_4$ nanoparticles (WF/$MnFe_2O_4$ and PF/$MnFe_2O_4$) were pipette out directly into three wells; and one well was filled with 100 µg/ml of the vehicle solvent DMSO. Following an incubation period of 24 h at 37 °C, the antimicrobial activity was evaluated by inhibition zones of bacterial growth.

Minimum inhibitory concentration

Minimum inhibitory concentration (MIC) is the lowest concentration of the antimicrobial agent that inhibits the microbial growth after 24-h incubation. MIC values of all the above tested pathogens were performed using standard broth micro dilution method with 96-well plates. The 12 wells of each row were filled with 0.5 ml sterilized Muller Hinton agar. Gentamicin (10 µg/ml) and Ketaconozole (10 µg/ml) were used as positive control for bacteria and fungus, respectively. Well 1 serve as growth control and well 12 serve as antibiotic control. The quantity of 0.5 ml of a mixture of culture medium and WF/$MnFe_2O_4$ and PF/$MnFe_2O_4$ NPs were added to wells 2–11 and it was diluted to create a concentration sequence from 0.512 to 0.008 ml. The deep wells were incubated for 24 h at 37 °C.

In vitro cytotoxicity activity

Human lung carcinoma (A549) and Human breast carcinoma (MCF-7) cell lines were used to evaluate the in vitro cytotoxic properties of newly synthesized $MnFe_2O_4$ NPs. Keratinocyte (HaCaT) cell line was used as normal cell line. MTT [3-(4,5-dimethylthiazol-2-yl)-2,5-diphenyltetrazolium bromide] assay was performed to access the cell viability. All the above cells were procured from NCCS (Natural Centre for Cell Science), Pune, India. The A549 cells were cultured in RPMI-1640 (Rosewell Park Memorial Institute), MCF-7 and HaCaT cells were cultured in DMEM (Dulbecco's Modified Eagles Medium). To ensure growth and viability of the cells, medium were supplemented with 10% FBS (Fetal bovine serum) and incubated in a humidified atmosphere with 5% CO_2 at 37 °C. HaCaT, A549 and MCF-7 cells were seeded separately at the concentration of 2.5×10^3 cells/well in 96 well plates and these cells were allowed to cohere overnight at 37 °C in a humidified atmosphere with 5% CO_2 for 24 h. The various concentrations of WF/$MnFe_2O_4$ and PF/$MnFe_2O_4$ nanoparticles were dissolved in DMSO and infused in the above process. After 24 h, MTT reagent [3-(4,5-dimethylthiazol-2-yl)-2,5-diphenyltetrazolium bromide] was added to each well and incubated at 37 °C for 4 h. The medium without the complex is served as control. To compare the results, anticancer activity of cisplatin was also evaluated under the same experimental conditions. Absorbance was recorded at 595 nm and sensitivity to cisplatin and the compounds were calculated based on cell proliferation measurements. The concentration required to kill 50% of the cell (IC_{50}) was also calculated.

Results and discussion

Structural analysis

The crystal structure and phase purity of the newly synthesized nanocrystalline spinel $MnFe_2O_4$ NPs were evaluated by X-ray diffraction (XRD). Figure 1a, b represents the XRD patterns of the sample synthesized via sol–gel method using wheat flour and potato flour, respectively. In Fig. 1a the diffraction peaks show the reflection planes (111), (202), (311), (222),(400),(333),(404), (440), (533) and (622) which match well with the standard diffraction values of JCPDS file no 74-2403 [26–30]. All these peaks confirm the cubic spinel lattice of $MnFe_2O_4$. This indicates that wheat flour (Fig. 1a) as surfactant led to the formation of $MnFe_2O_4$ particles of good crystallinity with no impurity phase. However, the XRD pattern of the sample has been synthesized with the surfactant potato flour (Fig. 1b) shows the peaks corresponding to spinel structure and additional peaks at 35.6° and 64.1° are due to α-Fe_2O_3.

The average crystallite size of the $MnFe_2O_4$ samples were calculated using Debye-Scherrer's formula

$$L = \frac{0.89\lambda}{\beta \cos\theta},$$

where L is the crystallite size, θ, the Bragg diffraction angle, λ, the X-ray wavelength and β, the full width at half maximum (FWHM). The average particle size of $MnFe_2O_4$ calculated from the diffraction peaks was found to be around 23 nm for WF/$MnFe_2O_4$ NP and 16 nm for PF/$MnFe_2O_4$ NP. It is clearly found that PF/$MnFe_2O_4$ NP is smaller when compared with WF/$MnFe_2O_4$.

The calculated lattice parameter was found to be 8.492 Å for WF/$MnFe_2O_4$ NP and 8.496 Å for PF/$MnFe_2O_4$ NP, which has good correlation with the JCPDS Card No 74-2403 and the calculated values of lattice parameter and crystallite size are given in Table 1.

Fourier transform infrared spectroscopy (FT-IR) studies

The functional group was investigated via Fourier Transform Infrared Spectroscopy (FT-IR) measurements. Figure 2 shows the FT-IR spectrum of $MnFe_2O_4$ samples. The two strong absorption peaks below 1000 cm^{-1} in both samples indicates the presence of ferrites [31]. The stretching between 400 and 700 cm^{-1} are the vibrations of (Fe–O) which are indicative of formation of spinel ferrite structure [31]. In ferrites the metal ions occupy two different

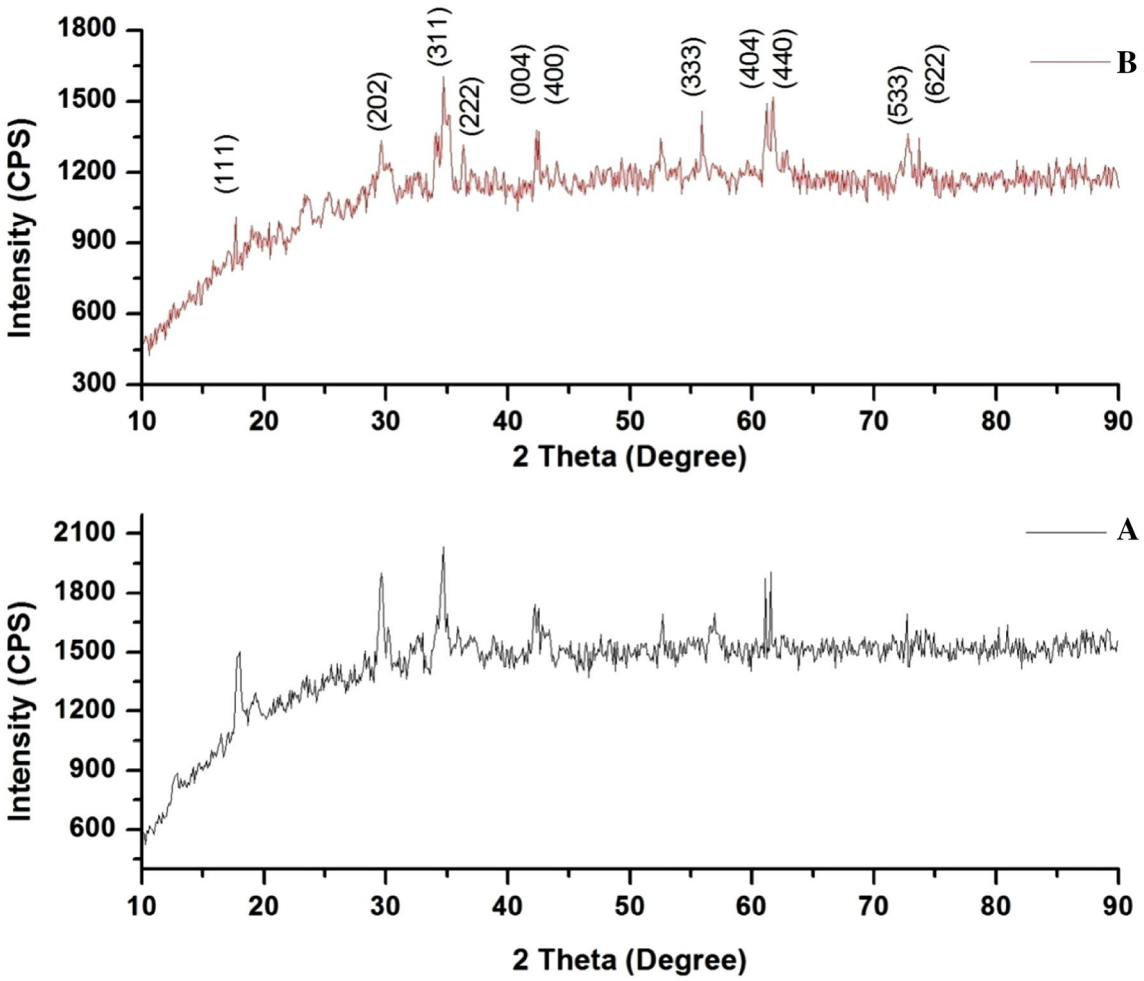

Fig. 1 XRD Patterns of $MnFe_2O_4$ synthesized using surfactant **a** wheat flour **b** potato flour

Table 1 XRD patterns of WF/$MnFe_2O_4$ and PF/$MnFe_2O_4$ nanoparticles

Samples	Crystallite size (nm)	Lattice parameter (Å)
Sample A (WF/$MnFe_2O_4$)	23.12	8.492
Sample B (PF/$MnFe_2O_4$)	16.87	8.496

interstitial sites in the lattice. One is at the tetrahedral site while the other is at the octahedral site [31, 32]. From the FT-IR spectra, it is found that high frequency bands at 875 cm^{-1} is associated to the tetrahedral site while the low frequency band at 629 cm^{-1} is associated to the octahedral site [31]. The sharpness of these bands is correlated to the high degree of crystallinity of $MnFe_2O_4$ nanostructures. A broad vibration band at 3449 and 3421 cm^{-1} are associated with the O–H stretching vibration of the adsorbed water molecules indicating higher amount of surface OH [33, 34]. A small band at 1383 cm^{-1} is assigned to the stretching vibrations of the COO group. A band at 1441 and 1449 cm^{-1} are assigned to C–H bending modes. The peaks at 1116 and 1110 cm^{-1} may be due to (C–O–C) symmetric vibration and dehydration of OH group from the polymers. The absence of peaks in the range of 2000–3000 cm^{-1} in the sample confirms the absence of O–H mode, C–O mode and C–H stretching mode.

Morphological analysis

Figure 3a, b shows the obtained SEM images of $MnFe_2O_4$ samples synthesized from wheat flour and potato flour. Both samples have been characterized by SEM microscopy to study their morphology, size, shape and agglomeration. The SEM image of PF/$MnFe_2O_4$ (Fig. 3b) reveals that the morphology of the particles was dispersed uniformly with a wider range of particle sizes, whereas grain growth was apparent in WF/$MnFe_2O_4$ (Fig. 3a). The particles were agglomerated due to interaction between magnetic nanoparticles. Heat treatment would have also caused agglomeration,

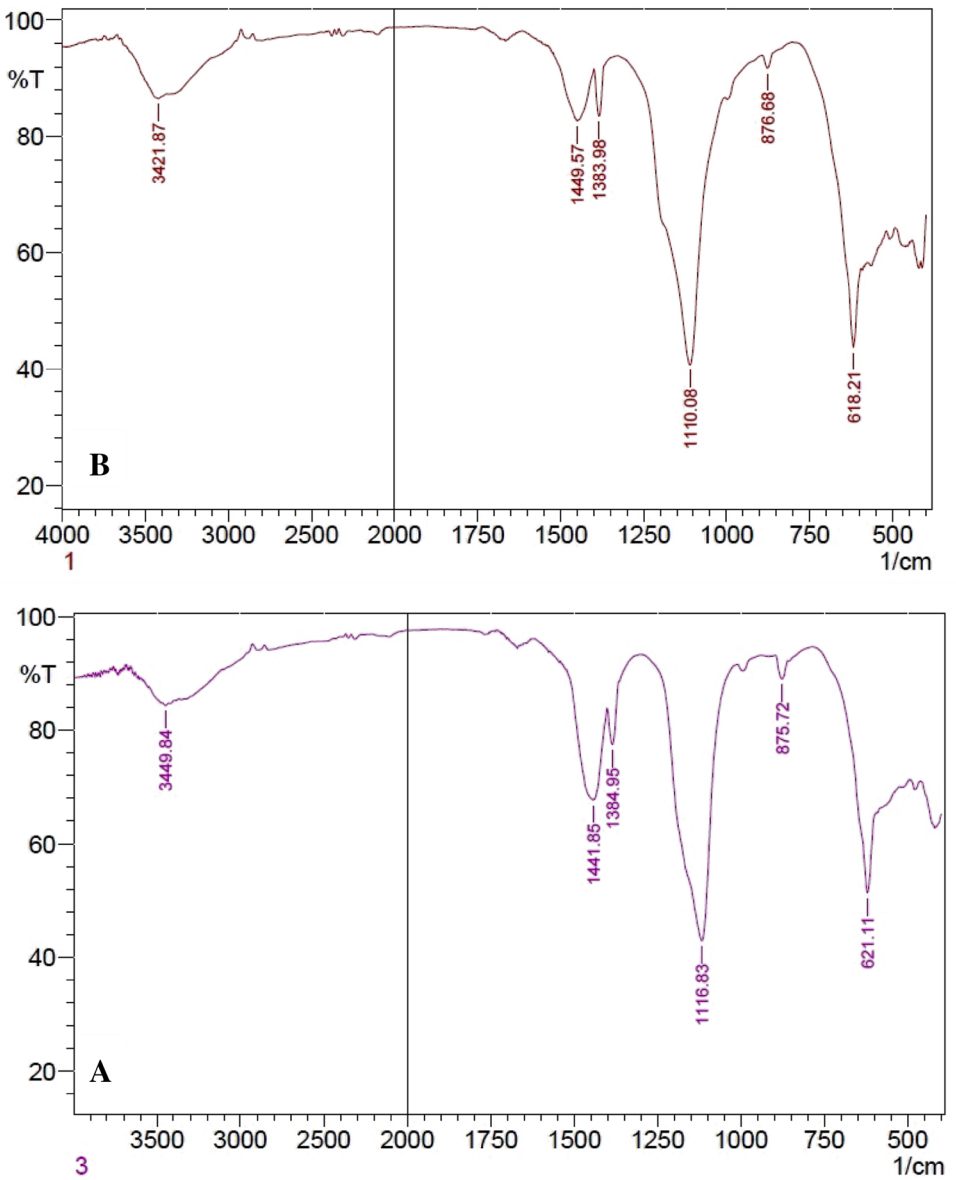

Fig. 2 FT-IR Spectra of $MnFe_2O_4$ synthesized using surfactant **a** wheat flour **b** potato flour

resulting in bigger grains. This is a typical characteristic feature of spinel ferrites [33, 35]. By analyzing both the samples, sample prepared using PF act as better surfactant than sample prepared using WF.

Energy dispersive X-ray (EDX) analysis

The elemental analysis and purity of $MnFe_2O_4$ nanocrystalline samples were confirmed by EDX analysis and the peaks obtained are shown in Fig. 4a, b. EDX results confirms the presence of Fe, Mn and O elements in $MnFe_2O_4$ samples. In addition to these peaks, a small peak is also found at 2.1 keV in both the samples, which indicates the presence of Au which has been used as a sputter coating, while preparing the samples for the analysis.

BET surface area

The surface adsorbance capability of $MnFe_2O_4$ nanoparticles were determined using Brunauer–Emmett–Teller (BET) surface area technique using N_2 adsorption/desorption studies. The surface area of PF/$MnFe_2O_4$ (75.76 m^2/g) was found to be higher than that of WF/$MnFe_2O_4$ (39.21 m^2/g). High surface area of PF/$MnFe_2O_4$ is due to the smaller particle size of the sample, which is confirmed by XRD and HR-SEM. From this it is expected that the high surface area of PF/$MnFe_2O_4$ could enhance the catalytic properties, than that of WF/$MnFe_2O_4$.

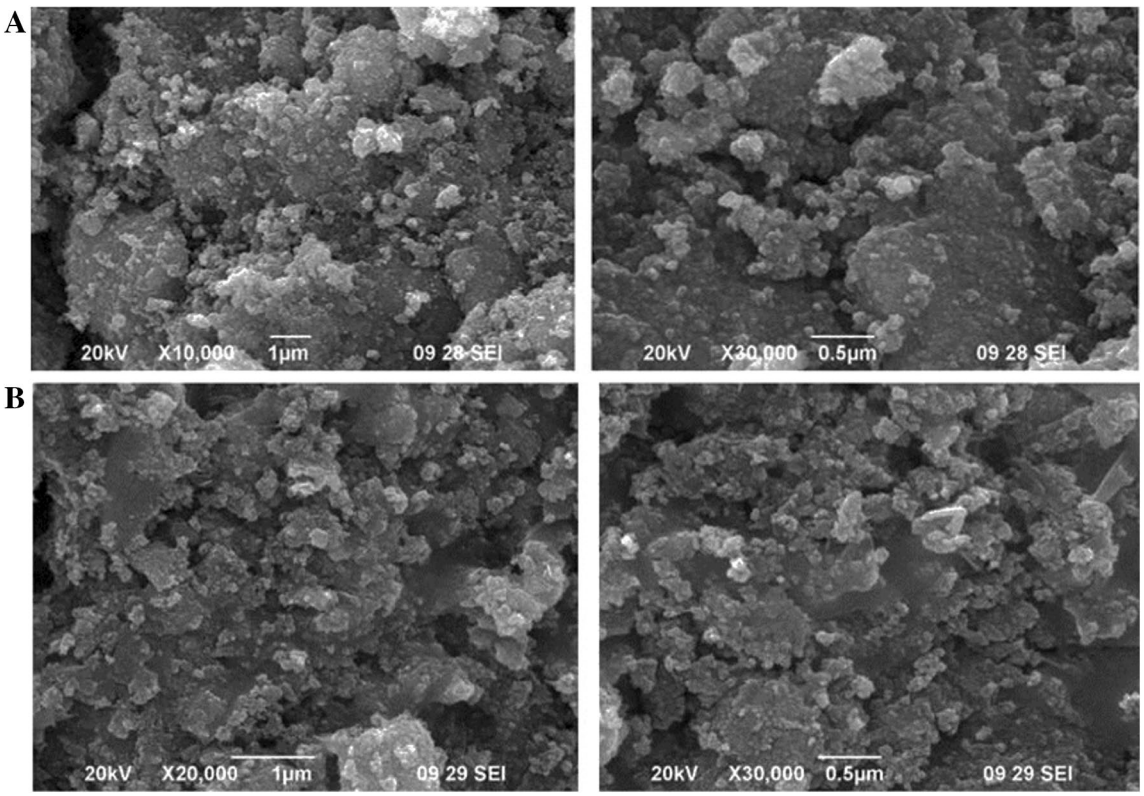

Fig. 3 SEM images of $MnFe_2O_4$ synthesized using surfactant **a** wheat flour **b** potato flour

Optical properties

Photoluminescence spectra gives information about luminescence properties. In addition to this it can also give the information of sub-band gap defect states of spinel $MnFe_2O_4$ nanoparticles. Figure 5 shows the absorption and emission spectra of spinel $MnFe_2O_4$ nanoparticles recorded at room temperature. Absorption peak observed in the range of 340–370 nm in both samples indicates the presence of defects and oxygen vacancies. A visible region peak observed at 412 and 413 nm is also attributed to the oxygen vacancies. Two peaks appeared around 412 and 413 nm corresponds to blue emission due to the radioactive defects related to the interface traps existing at the grain boundaries [36]. PL emission spectrum of $MnFe_2O_4$ samples shows maximum level at 412 nm (blue emission) which indicates the recombination of electrons deeply trapped in oxygen vacancies with photo generated holes [37]. The PL intensity of WF/$MnFe_2O_4$ NP for blue emission is approximately 1.1 times greater than that of PF/$MnFe_2O_4$. So $MnFe_2O_4$ sample synthesized using wheat flour as surfactant is found to have more defects and oxygen vacancies. But WF/$MnFe_2O_4$ with such defects may be preferred for luminescence devices, as its PL intensity is higher.

Magnetic properties

At room temperature, using Vibrating Sample Magnetometer (VSM) technique, the magnetic properties of spinel $MnFe_2O_4$ samples were recorded and the results of hysteresis are shown in Fig. 6. The obtained values of saturation magnetization (M_s), remnant magnetization (M_r) and coercivity (H_c) are given in Table 2 and the M–H loops of both the samples are given in Fig. 6. The samples exhibit a superparamagnetic behavior. M_s and H_c value of sample have been synthesis using wheat flour was found to be 45.23 emu/g and 67 Oe, whereas, it was reduced to 38.21 emu/g and 54 Oe of sample synthesis using potato flour [38–40]. The presence of α-Fe_2O_3 in PF/$MnFe_2O_4$ contributed to the decrease saturation magnetization value [41]. In general coercivity (H_c) of a magnetic material is a measure of its magneto crystalline anisotropy [42]. It seems to originate from the exchange anisotrophy due to spin disorder at the particle interface. This effect is expected to be larger for smaller particle size due to increase in surface-to-volume ratio [43].

Catalytic test

The catalytic oxidation of benzyl alcohol was studied using $MnFe_2O_4$ NPs as catalyst and the performance have been

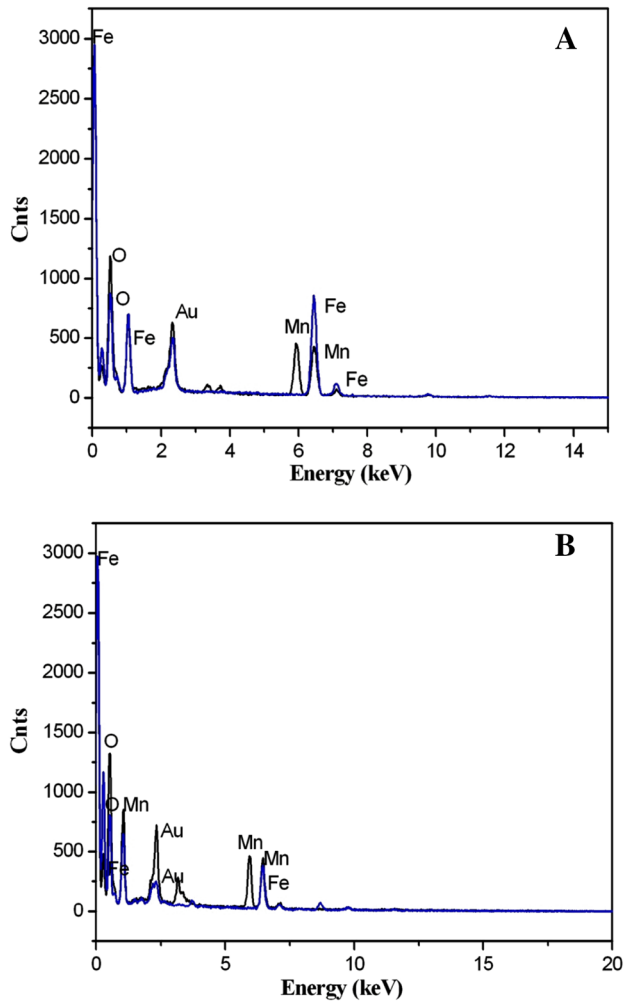

Fig. 4 EDX spectra of $MnFe_2O_4$ synthesized using surfactant **a** wheat flour **b** potato flour

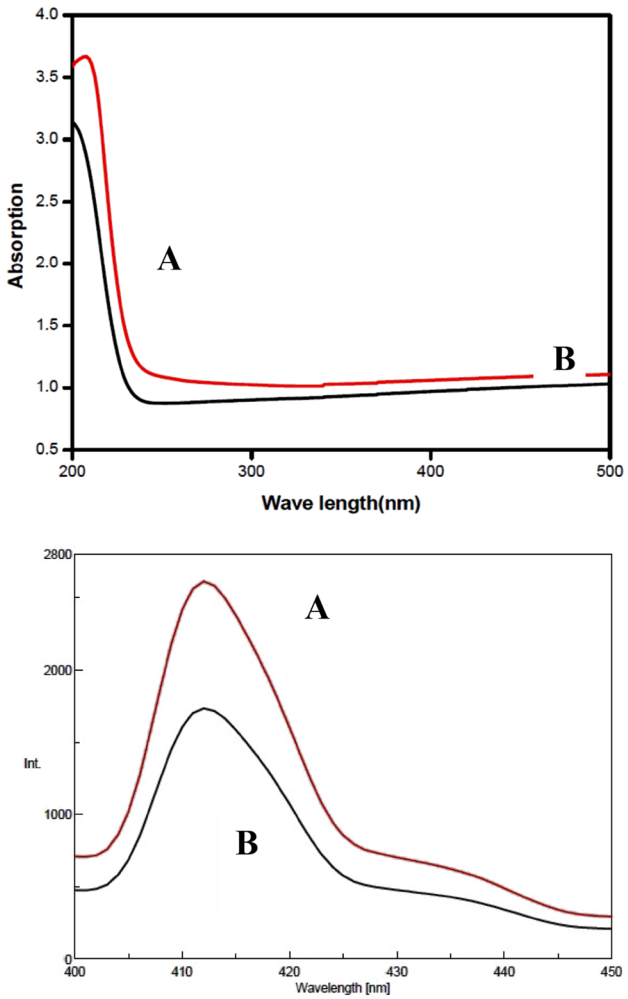

Fig. 5 UV and PL spectra of $MnFe_2O_4$ synthesized using surfactant **a** wheat flour **b** potato flour

investigated. Moreover, oxidized products were analyzed using gas chromatography (GC). Here the conversion reached a maximum of 89.47% for PF/$MnFe_2O_4$ and 68.79% for WF/$MnFe_2O_4$ and it is given in Table 3. The $MnFe_2O_4$ have been synthesized using potato flour as surfactant performed as good catalyst with higher yield of benzaldehyde. It is mainly due to small particle size with higher surface area of PF/$MnFe_2O_4$. This heterogeneous spinel $MnFe_2O_4$ catalyst is non-toxic, eco-friendly and has an excellent catalytic performance.

Antimicrobial activity

The antimicrobial test was performed on pathogenic organisms using spinel $MnFe_2O_4$ nanoparticles as an antimicrobial agent and their performance was investigated. The WF/$MnFe_2O_4$ and PF/$MnFe_2O_4$ NPs shows significant antibacterial and antifungal activity against all the organisms as given in Table 4. Both the sample controls all the test microorganisms performed in this study. Among these, *Streptococcus pneumoniae*, *Pseudomonas aeruginosa* and *Candida albicans* were found to be most sensitive. These pathogens are those which developed resistance to all the available antibiotics. From the results obtained, it is confirmed that, PF/$MnFe_2O_4$ shows the initial inhibition from 25 µg/ml for *Pseudomonas aeruginosa*, *Streptococcus pneumoniae* and *Candida albicans*. But there was no inhibition in 25 µg/ml with WF/$MnFe_2O_4$ for the tested pathogens. The antibacterial and antifungal activity results clearly shows that the zone of inhibition values against bacterial and fungal species produced by PF/$MnFe_2O_4$ were significantly higher than that of WF/$MnFe_2O_4$. In the zone of 50 and 100 µg/ml PF/$MnFe_2O_4$ shows higher inhibition than WF/$MnFe_2O_4$. Thus, PF/$MnFe_2O_4$ was most effective and shows a strong antibacterial and antifungal property against all the test pathogens. Hence, experiments were conducted to determine their

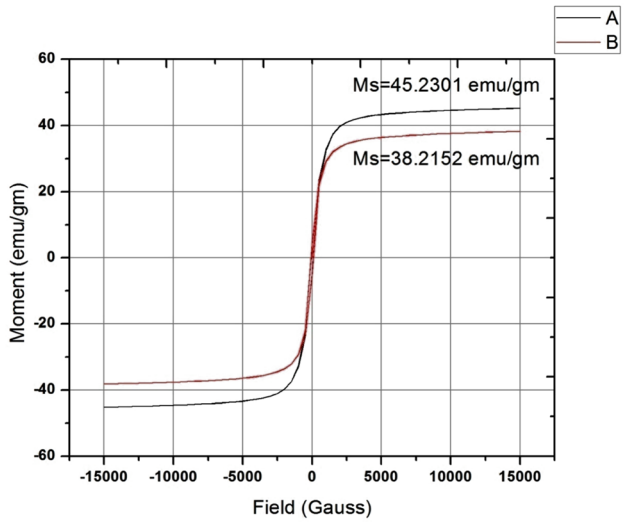

Fig. 6 Magnetic hysteresis (M–H) loops of $MnFe_2O_4$ synthesized using surfactant **a** wheat flour, **b** potato flour

Table 2 VSM measurements of WF/$MnFe_2O_4$ and PF/$MnFe_2O_4$ nanoparticles

Samples	M_s (emu/g)	M_r (emu/g)	H_c (Oe)
Sample A (WF/$MnFe_2O_4$)	45.23	4.36	54
Sample B (PF/$MnFe_2O_4$)	38.21	5.05	67

Table 3 Conversion percentage of catalytic oxidation of benzyl alcohol into benzaldehyde

Catalysts	Conversion (%)	Selectivity (%)
Sample A (WF/$MnFe_2O_4$)	68.79	100
Sample B (PF/$MnFe_2O_4$)	89.47	100

Minimum Inhibitory Concentration (MIC) and their results are reported in Table 5. The significant inhibition property of PF/$MnFe_2O_4$ might be due to its smaller particle size with high surface area.

Anticancer studies

The anti-proliferative activity of newly synthesized samples (WF/$MnFe_2O_4$ and PF/$MnFe_2O_4$) on human lung carcinoma (A549) and human breast carcinoma (MCF-7) were analyzed using MTT assay in a dose dependent fashion. It was compared with cisplatin (Fig. 7). The dose dependent cell death inducing ability of the compounds has been investigated using the percentage of cell viability verses complex concentration plot. New compounds which are synthesized revealed better reduction in the cell viability. The dose dependent cell inducing ability of the compounds on A549 and MCF-7 cell lines are shown in Figs. 8 and 9. Both samples show significant inhibition than cisplatin. Among these two samples, PF/$MnFe_2O_4$ shows better inhibition than WF/$MnFe_2O_4$. IC_{50} value of the cell lines are calculated and shown in Fig. 10. WF/$MnFe_2O_4$ and PF/$MnFe_2O_4$ NPs shows an IC50 value of 1.11, 1.18 µM against A549 and 1.32, 1.19 µM against MCF-7 cell lines, respectively. Figure 11 shows the cell inducing ability of normal HaCaT cell line. From the results obtained against human keratinocyte cell, it is concluded that both the samples were non-toxic to normal cell line.

Conclusions

WF/$MnFe_2O_4$ and PF/$MnFe_2O_4$ NPs were successfully synthesized by a simple sol–gel method using natural surfactants like wheat flour and potato flour. XRD results confirm pure cubic spinel crystalline structure for the sample synthesis using wheat flour. But potato flour had an

Table 4 *In vitro* antimicrobial activity of WF/$MnFe_2O_4$ and PF/$MnFe_2O_4$ NPs

Microbial pathogens		Zone of inhibition						
		Standard 10 µg/ml (S)	25 µg/ml		50 µg/ml		100 µg/ml	
			WF/$MnFe_2O_4$	PF/$MnFe_2O_4$	WF/$MnFe_2O_4$	PF/$MnFe_2O_4$	WF/$MnFe_2O_4$	PF/$MnFe_2O_4$
Gram-positive bacteria	*Staphylococcus aureus*	20.19 ± 0.40	–	–	15.44 ± 0.22	15.86 ± 0.54	16.76 ± 0.33	17.88 ± 0.11
	Streptococcus pneumoniae	21.43 ± 0.54	–	11.19 ± 0.32	14.43 ± 0.65	15.54 ± 0.33	17.79 ± 0.12	18.09 ± 0.19
Gram-negative bacteria	*Pseudomonas aeruginosa*	21.38 ± 0.76	–	11.87 ± 0.65	13.98 ± 0.55	14.58 ± 0.65	17.33 ± 0.24	18.38 ± 0.66
	Salmonella paratyphi	20.43 ± 0.55	–	–	14.39 ± 0.20	15.55 ± 0.40	17.44 ± 0.54	18.29 ± 0.11
Fungus	*Candida albicans*	21.55 ± 0.22	–	12.22 ± 0.65	13.33 ± 0.11	15.89 ± 0.34	17.38 ± 0.30	17.89 ± 0.66

Table 5 MIC values of WF/$MnFe_2O_4$ and PF/$MnFe_2O_4$ NPs for different microbial pathogens

Samples MIC (μg/ml)	Microbial pathogens				
	S. aureus	*S. pneumoniae*	*P. aeruginosa*	*S. typhi*	*C. albicans*
WF/$MnFe_2O_4$	31.78	29.10	31.35	28.22	24.83
PF/$MnFe_2O_4$	15.12	27.38	16.12	15.34	13.22

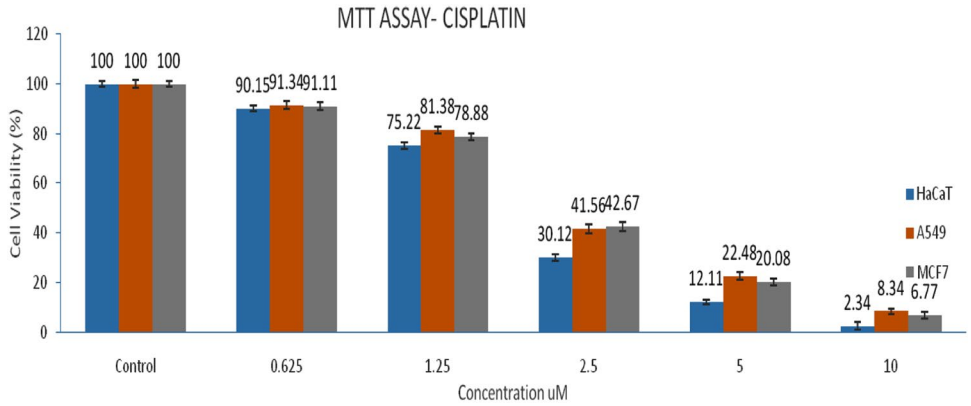

Fig. 7 Cytotoxicity effect of Cisplatin

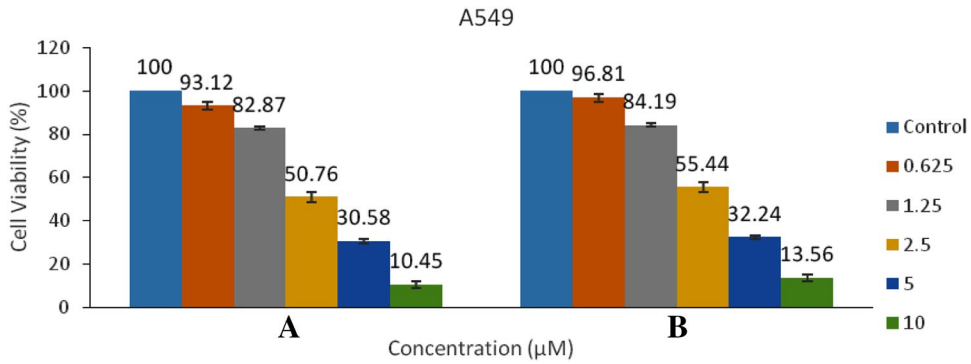

Fig. 8 Cytotoxic effect of WF/$MnFe_2O_4$ (**a**) and PF/$MnFe_2O_4$ (**b**) in A549 cells after 24-h post-incubation. Values are represented as mean ± SEM with triplicate estimations

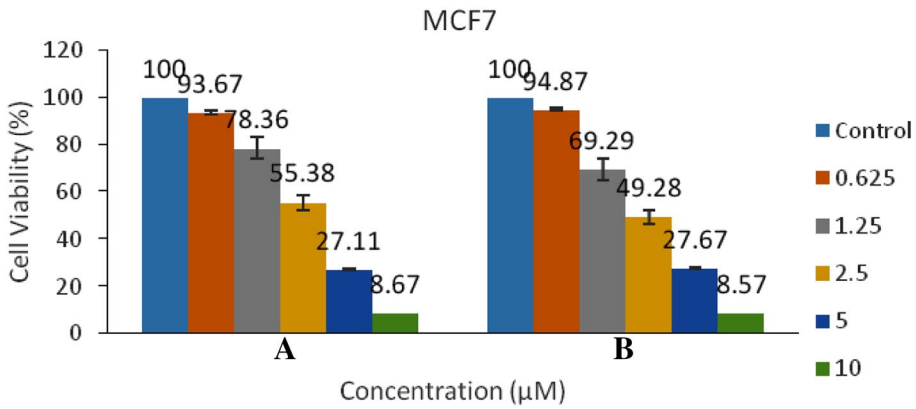

Fig. 9 Cytotoxic effect of WF/$MnFe_2O_4$ (**a**) and PF/$MnFe_2O_4$ (**b**) in MCF-7 cells after 24-h post-incubation. Values are represented as mean ± SEM with triplicate estimations

impurity phase of α-Fe_2O_3. The average crystallite size was calculated by Debye-Scherrer formula and it was found to be 23 nm for WF/$MnFe_2O_4$ and 16 nm for PF/$MnFe_2O_4$. SEM images show the morphology of the samples with well-defined nanoparticle structure with agglomeration. The surface area of PF/$MnFe_2O_4$ (75.76 m^2/g) was found to be higher than that of WF/$MnFe_2O_4$ (39.21 m^2/g). High surface area of PF/$MnFe_2O_4$ is due to the smaller particle size of PF/$MnFe_2O_4$. FT-IR study confirms the nature of

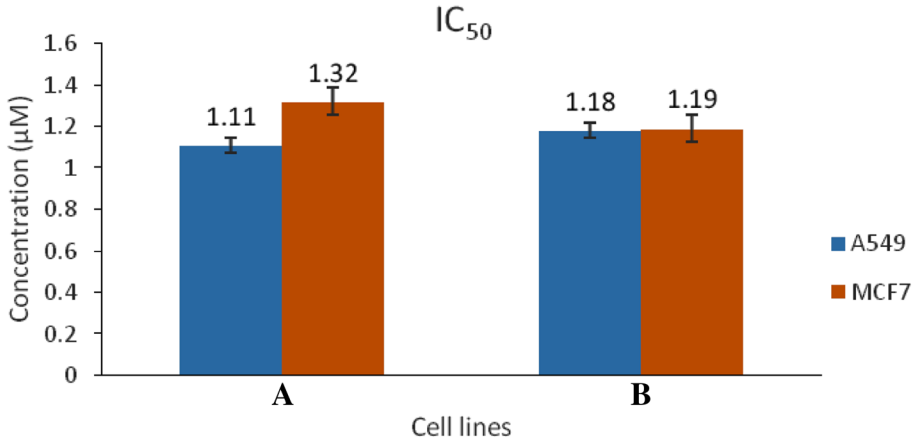

Fig. 10 IC_{50} values of WF/$MnFe_2O_4$ (**a**) and PF/$MnFe_2O_4$ (**b**) against A549 and MCF-7 cell lines

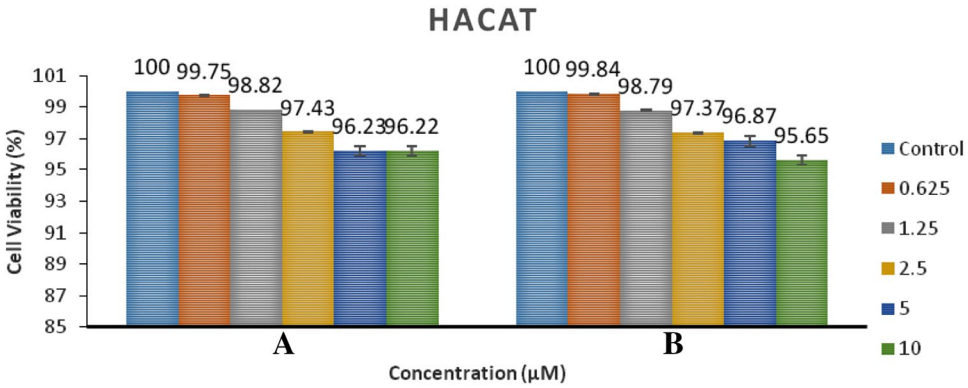

Fig. 11 Cytotoxic effect of WF/$MnFe_2O_4$ (**a**) and PF/$MnFe_2O_4$ (**b**) in HaCaT keratinocyte cells after 24-h post-incubation. Values are represented as mean ± SEM with triplicate estimations

bonds in synthesized ferrites. PL studies show a broad blue emission band for both the samples. VSM result shows the super-paramagnetic behavior to both the samples. The conversion of benzyl alcohol reached a maximum of 89.47% for $MnFe_2O_4$ synthesized using PF as surfactant, whereas for sample synthesized using wheat flour as surfactant, this conversion was only 68.79% with 100% selectivity. In the antimicrobial and antifungal test, PF/$MnFe_2O_4$ was found to be most effective and shows a strong antibacterial and antifungal property against two Gram-positive bacteria (*Staphylococcus aureus*, *Streptococcus pneumoniae*), two Gram-negative bacteria (*Pseudomonas aeruginosa*, *Salmonella paratyphi*) and *candida albicans* fungus than WF/$MnFe_2O_4$. The significant inhibition property of PF/$MnFe_2O_4$ is due to its smaller particle size with high surface area. In the anti-proliferative activity, the newly synthesized samples revealed a better reduction in the cell viability. Both samples exhibit significant inhibition than cisplatin. On comparing, PF/$MnFe_2O_4$ shows better inhibition than WF/$MnFe_2O_4$. From the results obtained against human keratinocyte cell, it is concluded that both the samples were non-toxic to normal cell line.

Acknowledgements The authors are very grateful to the Bharathiar University, Coimbatore, India.

Compliance with ethical standards

Conflict of interest The authors declare that they have no conflict of interest.

References

1. Logeswari, P., Silambrasan, S., Jayanthi, A.: Synthesis of silver nanoparticles using plants extract and analysis of their antimicrobial property. J. Saudi Chem. Soc. **19**, 311–317 (2015)
2. Burda, C., Chen, X., Narayanan, R., El-Sayed, M.A.: Chemistry and properties of nano crystals of different shapes. Chem. Rev. **105**, 1025–1102 (2005)

3. Thill, A., Zeyons, O., Spalla, O., Chauvat, F., Rose, J., Auffan, M.: Cytotoxicity of CeO_2 nanoparticles for *Escherichia coli*, physico-chemical insight of the cytotoxicity mechanism. Environ. Sci. Technol. **40**, 6151–6156 (2006)
4. Apperlot, G., Lipovsky, A., Dror, R., Perkas, N., Nitzan, Y., Lubart, R.: Enhanced anti bacterial activity of nanocrystalline ZnO due to increased ROS-mediated cell injury. Adv. Funct. Mater. **19**, 842–852 (2009)
5. Shankar, B., Krishnan, S., Vasantha, M., Arun, B., Williams, P.H.: Outer membrane proteins of wild-type and intimin-deficient enteropathogenic *Escherichia coli* induce Hep-2 cell death through intrinsic and extrinsic pathways of apoptosis. Int. J. Med. Microbiol. **299**, 121–132 (2009)
6. Giri, A., Goswami, N., Sasmal, C., Polley, N., Majumdar, D., Sarkar, S., Bandyopadhyay, S.N., Singha, A., Pal, S.K.: Unprecedented catalytic activity of Mn_3O_4 nanoparticles: potential lead of a sustainable therapeutic agent for hyperbilirubinemia. RSC Adv. **4**(10), 5075–5079 (2014)
7. Pal, M., Lee, S., Kwon, D., Hwang, J., Lee, H., Hwang, S., Jeon, S.: Direct immobilization of antibodies on Zn-doped Fe_3O_4 nanoclusters for detection of pathogenic bacteria. Anal. Chim. Acta **952**, 81–87 (2017)
8. Hastings, J.M., Corliss, L.M.: Neutron diffraction study of manganese ferrite. Phys. Rev. **104**, 328–331 (1956)
9. Elfalaky, A., Soliman, S.: Theoretical investigation of $MnFe_2O_4$. J. Alloys Compd. **580**, 401–406 (2013)
10. Li, J., Yuan, H., Li, G., Li, Y., Leng, J.: Cation distribution dependence of magnetic properties of sol–gel prepared $MnFe_2O_4$ spinel ferrite nanoparticles. J. Magn. Magn. Mater. **322**, 3396–3400 (2010)
11. Pradhan, P., Giri, J., Samanta, G., Sarma, H.D., Mishra, K.P., Bellare, J.R., Banerjee, R., Bahadur, D.: Comparative evaluation of heating ability and biocompatibility of different ferrite based magnetic fluids for hyperthermia application. J. Biomed. Mater. Res. B **81B**, 12–22 (2007)
12. Pal, M., Singh, A.K., Rakshit, R., Mandal, K.: Facile functionalization of Fe_2O_3 nanoparticles to induce inherent photoluminescence and excellent photocatalytic activity. Appl. Phys. Lett. **104**, 233110 (2014)
13. Pal, M., Kundu, A., Rakshit, R., Mandal, K.: Surface chemistry modulated introduction of multifunctionality within Co_3O_4 nanocubes. RSC Adv. **5**(21), 16311–16318 (2015)
14. Pal, M., Kundu, A., Rakshit, R., Mandal, K.: Ligand induced evolution of intrinsic fluorescence and catalytic activity from cobalt ferrite nanoparticles. Chem. Phys. Chem. **8**(16), 1627–1634 (2015)
15. Chen, D., Zhang, Y., Kang, Z.: A low temperature synthesis of $MnFe_2O_4$ nanocrystals by microwave-assisted ball-milling. Chem. Engg. J. **215**, 235–239 (2013)
16. Singh, M., Sud, S.P.: Controlling the properties of magnesium–manganese ferrites. Mater. Sci. Eng. B **83**, 180–184 (2001)
17. Lakshman, A., Rao, K.H., Mendiratta, R.G.: Magnetic properties of In^{3+} and Cr^{3+} substituted Mg–Mn ferrites. J. Magn. Magn. Mater. **250**, 93–97 (2002)
18. Wolski, W., Wolska, E., Kaczmarek, J., Piszora, P.: Formation of manganese ferrite by modified hydrothermal method. Phys. Status Solidi **152**, 19–22 (1995)
19. Pal, M., Rakshit, R., Mandal, K.: Surface modification of $MnFe_2O_4$ nanoparticles to impart intrinsic multiple fluorescence and novel photocatalytic properties. ACS Appl. Mater. Interfaces **6**(7), 4903–4910 (2014)
20. Kurtan, U., Guner, A., Amir, M.D., Baykal, A.: Enhanced antibacterial performance of Fe_3O_4–Ag and $MnFe_2O_4$–Ag nanocomposites. Bull. Mater. Sci. **40**(1), 147–155 (2017)
21. Chitra, K., Reena, K., Manikandan, A., Arul Antony, S.: Antibacterial studies and effect of poloxamer on gold nanoparticles by zingiber officinale extracted green synthesis. J. Nanosci. Nanotechnol. **15**(7), 4984–4991 (2015)
22. Ferlay, J., Shin, H.R., Bray, F., Forman, D., Mathers, C., Parkin, D.: Estimates of worldwide burden of cancer in 2008. Int. J. Cancer **127**, 2893–2897 (2010)
23. Wei, Y., Xu, Y., Han, X., Qi, Y., Xu, L., Xu, Y., et al.: Anticancer effects of dioscin on three kinds of human lung cancer cells through inducing DNA damage and activating mitochondrial signal pathway. Food Chem. Toxicol. **59**, 118–128 (2013)
24. Akhtar, M., Swamy, M.K., Umar, A., Sahli, A., Abdullah, A.: Biosynthesis and characterization of silver nanoparticles from methanol leaf extract of *Cassia didymobotyra* and assessment of their antioxidant and antibacterial activities. J. Nanosci. Nanotechnol. **15**, 9818–9823 (2015)
25. Swamy, M.K., Akhtar, M.S., Mohanty, S.K., Sinniah, U.R.: Synthesis and characterization of silver nanoparticles using fruit extract of *Momordica cymbalaria* and assessment of their in vitro antimicrobial, antioxidant and cytotoxicity activities. Spectrochim. Acta. Mol. Biomol. Spectroc. **151**, 939–944 (2015)
26. Kozissnik, B., Bohorquez, A.C., Doboson, J., Rinaldi, C.: Magnetic fluid hyperthermia: advances, challenges and opportunity. Int. J. Hyperth. **29**, 706–714 (2013)
27. Guner, S., Amir, M.D., Geleri, M., Sertkol, M., Baykal, A.: Magneto-optical properties of Mn^{3+} substituted Fe_3O_4 nanoparticles. Ceram. Int. **41**, 10915–10922 (2015)
28. Amir, M.D., Unal Sagar, B., Shirsath, E., Geleri, M., Sertkol, M., Baykal, A.: Polyol synthesis of Mn^{3+} substituted Fe_3O_4 nanoparticles: cation distribution, structural and electrical properties. Superlattice Microstruct. **85**, 747–760 (2015)
29. Mary Jacintha, A., Manikandan, A., Chinnaraj, K., Arul Antony, S., Neeraja, P.: Comparative studies of spinel $MnFe_2O_4$ nanostructures: structural, morphological, optical, magnetic and catalytic properties. J. Nanosci. Nanotechnol. **15**, 9732–9740 (2015)
30. Amir, M.D., Kurtan, U., Baykal, A., Sozeri, H.: $MnFe_2O_4$@PANI@Ag heterogeneous nanocatalyst for degradation of industrial aqueous organic pollutants. J. Mater. Sci. Technol. **32**, 134–141 (2016)
31. Seema, J., Manoj, K., Sandeep, C., Geetika, S., Mukesh, J., Singh, V.N.: Structural, magnetic, dielectric and optical properties of nickel ferrite nanoparticles synthesized by coprecipitation method. J. Mol. Struct. **55**, 1076–1081 (2014)
32. Nandhini, J., Neeraja, P., Rex Jeya Rajkumar, S., Umapathy, V., Suresh, S.: Comparative studies of microwave and sol–gel-assisted combustion methods of $NiFe_2O_4$ nanostructures: synthesis, structural, morphological, opto-magnetic and antimicrobial activity. J. Supercond. Nov. Magn. **30**, 1213–1220 (2017)
33. Jacintha, M., Neeraja, P., Sivakumar, M., Chinnaraj, K.: Comparative study of $MnFe_2O_4$ nanoparticles synthesized by sol–gel method with two different surfactants. J. Supercond. Nov. Magn. **30**, 237–242 (2017)
34. Li, K., Cheng, R., Wang, S., Zhang, Y.: Infrared transmittance spectra of the granular perovskite. J. Phys. Condens. Matter **10**, 4315–4319 (1998)
35. Gharagozlou, M.: Synthesis, characterization and influence of calcination temperature on magnetic properties of nanocrystalline spinel Co-ferrite prepared by polymeric precursor method. J. Alloy Compd. **486**, 660–665 (2009)
36. Zang, C.H., Zhang, D.M., Tang, C.J., Fang, S.J., Zong, Z.J., Yang, Y.X., Zhao, C.H., Zhang, Y.S.: Optical properties of a ZnO/P nanostructure fabricated by a chemical vapour deposition method. J. Phys. Chem. **113**, 18527–18530 (2009)
37. Bhargava, R., Sharma, P.K., Dutta, R.K., Kumar, S., Pandey, A.C., Kumar, N.: Influence of Co-doping on the thermal, structural and optical properties of sol–gel derived ZnO nanoparticles. Mater. Chem. Phys. **120**, 393–398 (2010)

38. Stoia, M., Muntean, E., Păcurariu, C., Mihali, C.: Thermal behavior of $MnFe_2O_4$ and $MnFe_2O_4$/C nanocomposite synthesized by a solvothermal method. Thermochim. Acta **652**, 1–8 (2017)
39. Güner, S., Amir, M., Geleri, M., Sertkol, M., Baykal, A.: Magneto-optical properties of Mn^{3+} substituted Fe_3O_4 nanoparticles. Ceram. Int. **41**, 10915–10922 (2015)
40. Topkaya, R., Kurtan, U., Baykal, A., Toprak, M.S.: Polyvinylpyrrolidone (PVP)/$MnFe_2O_4$ nanocomposite: sol–gel autocombustion synthesis and its magnetic characterization. Ceram. Int. **39**, 5651–5658 (2013)
41. Rivas, P., Sagredo, V., Rossi, F., Pernechele, C., Solzi, M., Pena, O.: Structural, magnetic and optical characterization of $MnFe_2O_4$ nanoparticles synthesized via sol–gel method. IEEE Trans. Magn. **49**, 4568–4571 (2013)
42. Joy, P.A., Date, S.K.: Effect of sample shape on the zero-field cooled magnetization behavior: comparative studies on $NiFe_2O_4$, $CoFe_2O_4$ and $SrFe_2O_4$. J. Magn. Magn. Mater. **222**, 33–38 (2000)
43. Kasapoglu, N., Baykal, A., Koseoglu, Y., Toprak, M.S.: Microwave-assisted combustion synthesis of $CoFe_2O_4$ with urea and its magnetic characterization. Scr. Mater. **57**, 441–444 (2007)

Affiliations

A. Mary Jacintha[1,2] · V. Umapathy[3] · P. Neeraja[4] · S. Rex Jeya Rajkumar[5]

✉ P. Neeraja
researchneeraja@gmail.com

[1] Research and Development Centre, Bharathiar University, Coimbatore 641 046, India

[2] Department of Chemistry, Varuvan Vadivelan Institute of Technology, Dharmapuri 636 703, India

[3] Caplin Point Laboratories Ltd, Chennai 600017, India

[4] Department of Chemistry, Government Arts and Science College, Hosur 635109, India

[5] Department of Bioscience and Technology, Karunya University, Coimbatore 641114, India